Light-induced states in attosecond transient absorption spectra of laser-dressed helium

Shaohao Chen,[1,*] M. Justine Bell,[2,3,*] Annelise R. Beck,[2,3] Hiroki Mashiko,[2] Mengxi Wu,[1] Adrian N. Pfeiffer,[2,3] Mette B. Gaarde,[1] Daniel M. Neumark,[2,3] Stephen R. Leone,[2,3,4] and Kenneth J. Schafer[1]

[1]*Department of Physics and Astronomy, Louisiana State University, Baton Rouge, Louisiana 70803, USA*

[2]*Ultrafast X-ray Science Laboratory, Chemical Sciences Division, Lawrence Berkeley National Laboratory, Berkeley, California 94720, USA*

[3]*Department of Chemistry, University of California, Berkeley, California 94720, USA*

[4]*Department of Physics, University of California, Berkeley, California 94720, USA*

(Received 5 September 2012; revised manuscript received 26 November 2012; published 17 December 2012)

Laser-dressed absorption in atomic helium is studied, both theoretically and experimentally, by transient absorption spectroscopy using isolated 400-as pulses centered at 22 eV and 12-fs near-infrared (NIR) pulses with 780-nm central wavelength. Multiple features in the helium singly excited bound-state spectrum are observed only when the NIR and attosecond pulses are overlapped in time. Theoretical analysis indicates that these light-induced structures (LISs) are the intermediate states in resonant, second-order processes that transfer population to multiple dipole forbidden states. The use of broadband, coherent extreme ultraviolet (XUV) radiation allows observation of these LISs without specifically tuning to a two-photon resonance, as would be required with narrowband XUV light. The strength and position of the LISs depend strongly on the NIR intensity and the pump-probe delay.

DOI: 10.1103/PhysRevA.86.063408 PACS number(s): 32.80.Rm, 32.70.Jz, 42.50.Hz, 42.50.Md

Attosecond transient absorption spectroscopy provides numerous opportunities for the design of experiments that take advantage of the complex interactions between an isolated attosecond pulse (IAP), a strong laser field, and a target medium [1–4]. Of particular interest are nonlinear processes that combine the IAP and laser fields. Nonlinear coupling schemes, such as those associated with laser-dressed absorption, are powerful tools in many disciplines for creating state-selected populations and aligned molecules [5], modifying optical properties of media (for example, causing transparency [6]), and processing quantum information [7].

This joint experimental and theoretical study focuses on the time-resolved absorption of IAPs by helium atoms at energies between 20 and 24 eV in the presence of a delayed near infrared (NIR) pulse. When the IAP and NIR pulses overlap, several new features in the transient absorption spectra below the single ionization threshold are observed which are not associated with any dipole-allowed extreme ultraviolet (XUV)–driven transition. Theoretical investigation reveals that each of these light-induced structures (LISs) involves the transfer of population from the ground $1s^2$ state to $1sns$ or $1snd$ states via resonant second-order processes requiring both the XUV and the NIR fields. In our experiment, the broad bandwidth of the IAP allows the simultaneous observation of all the LISs for each delay where the two fields are overlapped. As the NIR intensity or the NIR-IAP delay is changed, the light-induced states are observed to shift in energy and absorption strength, in agreement with the calculations.

Most previous absorption studies on laser-dressed He have been carried out with attosecond pulse trains (APTs). Modification of the ionization probabilities [8,9] and the absorption [10,11] as a function of NIR-APT delay has been observed for APTs overlapped in time with NIR fields. Additional work with APTs has considered the sensitive dependence of the ionization probability on the XUV wavelength chosen to resonantly excite specific $1snp$ states of He [12,13]. Recent work on transient IAP absorption in He focused on the subcycle changes in the linear XUV absorption around the $1s3p$ and $1s4p$ dipole allowed states [14]. This is in contrast to the work reported here, where multiple, resonant second-order transitions are observed and theoretically understood across the large bandwidth of the IAP.

The experimental setup is shown in Fig. 1. The IAPs are generated in krypton gas via double optical gating and spectrally limited to 20–24 eV by a 200-nm-thick Sn filter [15,16]. They are then are overlapped with a 12-fs, 780-nm NIR pulse in the absorption cell of an attosecond transient absorption spectrometer with a variable time delay between the pulses. In the absorption spectrometer, the NIR and IAP pulses are collinearly focused by a Ru-Si multilayer mirror ($f = 25$ cm) in a 1-mm-long target gas cell, filled with 20 Pa He. Transmitted XUV light is recollected by a Mo-Si multilayer mirror ($f = 25$ cm) and directed through an additional 200-nm Sn filter and onto the entrance slit of the XUV spectrometer. A gold-coated aberration-corrected grating spectrally disperses the IAP onto an x-ray charge-coupled device (CCD) camera, where the transmitted spectrum is recorded. The XUV spectrometer resolution is 100 meV, as determined from measurement of $1s2p$ and $1s3p$ He absorption lines.

The 400-as IAPs are characterized by photoelectron streaking [17,18], while the NIR pulse is measured by the spectral phase interferometry for direct electric field reconstruction (SPIDER) method [19]. For streaking, Kr gas is ionized by the IAP and overlapped with the NIR pulse, and a Ru-Si multilayer mirror is used to combine the two pulses. The principal component generalized projections algorithm [18,20] is used to reconstruct the pulses and, upon convergence, the extracted duration is 376 ± 7 as. The XUV pulses are not transform limited—the spectral phase of the attosecond pulse varies by approximately one radian across the pulse.

Transient absorption spectra are recorded as the average of five pump-probe scans, each of which is acquired for 30 000 laser pulses at every pump-probe time delay point. Absolute optical density (OD) spectra are constructed as

$$\mathrm{OD} = -\log[I_{\mathrm{sample}}(E)/I_0(E)], \quad (1)$$

[*]These authors contributed equally to this work.

 ©2012 American Physical Society

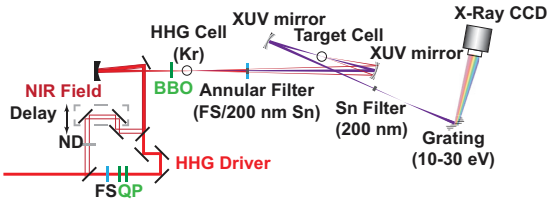

FIG. 1. (Color online) Experimental setup. Schematic of attosecond transient absorption instrument. ND, neutral density filters; FS, fused silica; and QP, quartz plates. Optics for double optical gating are shown in green (light gray). IR beam paths are shown in red (dark gray). IAP is shown in purple (gray).

where $I_{\text{sample}}(E)$ is the measured spectral intensity of the IAP after it passes through the 1-mm-long sample cell filled with 20 Pa He, and $I_0(E)$ is the spectral intensity of the IAP after it passes through the empty sample cell. To obtain a broad overview of the onset and evolution of the LISs, time delay scans over tens of femtoseconds are required. To that end, delay steps of ≈1.3 fs (one-half NIR cycle) were used in the experiment.

The theoretical treatment of laser-dressed absorption is based on the semiclassical picture of a quantum atom driven by a classical field [21,22]. We calculate the single-atom frequency-dependent response function:

$$\tilde{S}(\omega) = 2\,\mathrm{Im}\,[\tilde{d}(\omega)\tilde{\mathcal{E}}^*(\omega)], \tag{2}$$

where $\tilde{d}(\omega)$ is the Fourier transform of the dipole moment $d(t)$, obtained by solving the time-dependent Schrödinger equation (TDSE) using the full IAP + NIR electric field $\mathcal{E}(t)$ in the single-active-electron approximation. Details of the method are given in Ref. [22]. Calculating the response nonperturbatively is advantageous because the atom exchanges energy with the light field over a large range of frequencies in many different orders of nonlinearity. The calculations treat all of these processes on an equal footing. For positive frequencies, $\omega\tilde{S}(\omega)$ is the energy gained or lost per unit frequency by the atom, meaning that positive or negative values of $\tilde{S}(\omega)$ represent absorption or emission at frequency ω. In this paper, we concentrate on absorption, which dominates the response.

The calculation of the energy exchange between the atom and the field requires a time scale for the decay of the dipole initiated by the driving fields. In an experiment, dephasing (collisional broadening, for example), spontaneous decay, and finite spectrometer resolution all serve to define effective time scales for the dipole decay. In the calculations these processes are absent and a numerical dephasing time is provided instead, by multiplying a smooth window function onto the calculated time-dependent dipole moment before Fourier transforming it to obtain the response function. In the work presented here we are primarily interested in the modification of the absorption by the NIR field, and using a dephasing time that is much longer than the NIR pulse duration is therefore sufficient. The 65-fs dephasing time used in this work gives a minimum spectral bandwidth of 20 meV. Doubling the dephasing time in the calculations does not change any of the conclusions presented below.

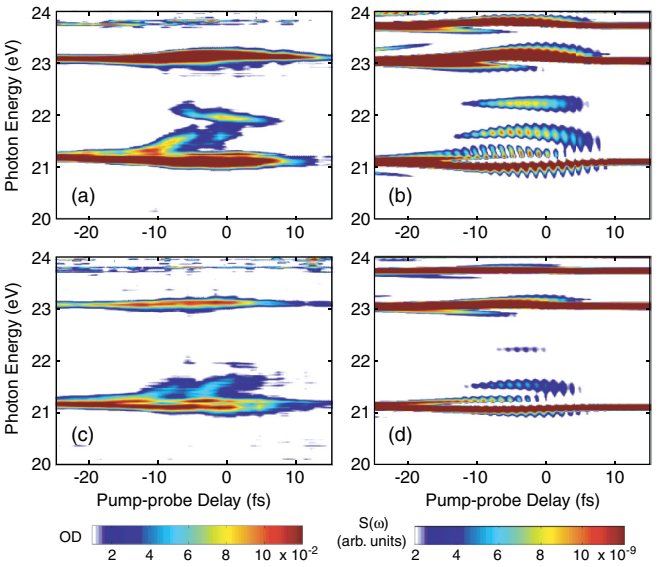

FIG. 2. (Color online) Experimental transient absorption spectra (left panels) and calculated single-atom frequency-dependent response (right panels) as a function of pump-probe delay. Negative delays indicate that the NIR pulse follows the IAP. The peak NIR intensities are (a), (b) 1.6×10^{12} W/cm^2 and (c), (d) 4.8×10^{11} W/cm^2. The theoretical plots use a small, nonzero value of the minimum response to better mimic the experiment. The $1s2p$ resonance is at 21.21 eV and the $1s3p$ resonance is at 23.09 eV.

A full theoretical treatment of transient absorption requires solving the Maxwell wave equation (MWE) for the time propagation of the light fields through the atomic medium. This is done using polarization and ionization source terms in the MWE that are obtained by solving the single-atom TDSE [22]. Coupling the MWE and TDSE solvers in this fashion requires much more numerical effort than the calculation of the single-atom response alone. A calculation of the full propagated light fields for XUV and NIR pulses that are overlapped with zero time delay and a pressure of 400 Pa shows that even though there is strong absorption, the time structure of the IAP is remarkably robust and does not undergo reshaping, only a small time shift of a few attoseconds. Repeating this calculation for several XUV-NIR time delays near zero shows that the macroscopic absorption spectra obtained from the full propagated light fields are similar in all their features to the single-atom results, scaled by the density. This means that it is sufficient to calculate the single-atom response in order to understand the experimental results.

Figure 2 shows experimental measurements (left panels) of the transient absorption of atomic He and compares them to theoretical calculations (right panels) of the frequency-dependent response function, both versus the NIR-IAP delay. Measurements were made using two NIR intensities estimated from *in situ* streaking shifts to be 1.6×10^{12} W/cm^2 and 4.8×10^{11} W/cm^2 [Figs. 2(a) and 2(c), respectively]. The intensity of the NIR field is controlled by a neutral density filter. Using the intensity profile of the NIR focus (measured with a CCD) and XUV focal spot size (calculated as twice the beam waist with standard Gaussian optical techniques) the NIR intensity is estimated to vary by 20% across the XUV focal spot. The theoretical calculations were made for the same peak

intensities using 12-fs transform-limited pulses with a central wavelength of 780 nm [Figs. 2(b) and 2(d)]. The delay step in the calculations is 0.16 fs. The overall agreement between experiment and theory is very good. Many of the features presenting only near zero delay are in notable accord, and features visible over the whole range of time delays are also reproduced.

In Fig. 2, delay times of $\tau_d > 10$ fs correspond to the NIR pulse arriving well before the IAP. Here, the absorption spectra comprise only resonant features due to excitation of the $1snp$ states by first-order XUV processes, identical to the case when no NIR is present. The NIR field is not strong enough to excite the atom out of its ground state. Because the instrumental resolution in the experiment is much larger than the Doppler broadened linewidth, the measured absorption resonances are observed as peaks of the same area spread over a larger spectral range. This implies that absorption of the XUV photons on resonance is much higher than expected from measured optical densities. In contrast, the absorption spectra are strongly modified when the XUV and NIR pulses overlap (-15 fs $< \tau_d < 10$ fs). Most striking is the enhanced absorption at frequencies that cannot be assigned to any linear XUV absorption process that reaches a field-free atomic state. Some of these LISs appear at energies between 21.25 and 22.5 eV in Fig. 2, energies that are distinct from the XUV-driven dipole allowed transitions to the $1s2p$ and $1s3p$ states.

For delays of $\tau_d < -15$ fs the calculations show several delay-dependent sidebands around the $1s2p$ absorption feature. These sidebands are due to perturbed free polarization decay [23], caused by the modulation of the $1s^2$-$1s2p$ coherence by the NIR pulse which arrives after the XUV has excited the system. The delay-dependent side bands are spaced as the reciprocal of the pump-probe delay, which is quite a bit smaller than the experimental resolution for large delay times. Although the sidebands are not observed in the experimental absorption spectra, the absorption strength appears to broaden and increase in this region; the broadening is real, but the absorption increase could be due to detector saturation on line center. Because of the finite spectrometer resolution, the limited number of XUV photons, and the strong and narrow lines of the He, the line centers can appear as if there is total absorption on some CCD camera pixels, with concurrent broadening of the features to adjacent pixels due to the wings of the lines. These complications can make precise comparison of the absolute intensities with theory difficult.

Figure 3 provides an intuitive interpretation of the light-induced structures near zero delay in the transient absorption spectra. Line spectra for both NIR intensities, measured at one pump-probe delay (-2.7 fs), are plotted in Fig. 3(a), with dashed lines indicating peak positions occurring in the 1.6×10^{12} W/cm^2 intensity spectrum. The position of the LISs suggests the interpretation diagramed in Fig. 3(b), where we assume that the strongest modification to the XUV absorption spectrum will be due to first-order NIR processes. Resonant processes are possible if the combination of XUV and NIR fields can couple the ground $1s^2$ state to $1sns$ or $1snd$ states. The LISs in the absorption spectrum are then interpreted—in the frequency domain—as the intermediate states of processes that involve the absorption or emission

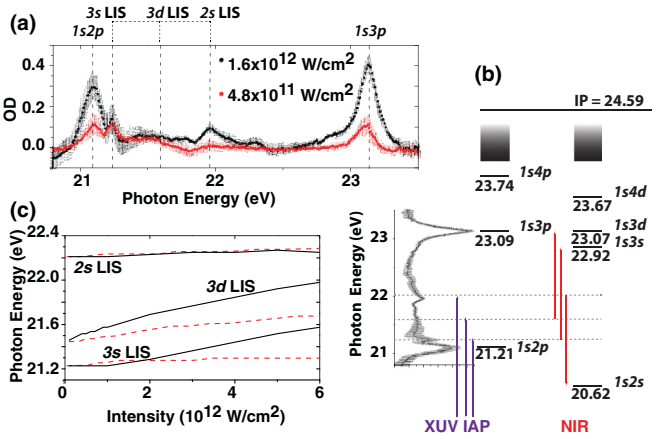

FIG. 3. (Color online) Experimental transient absorption spectra. (a) Line spectra at a pump-probe delay of -2.7 fs for intensities of 1.6×10^{12} W/cm^2 (black) and 4.8×10^{11} W/cm^2 (red [gray]). Error bars represent $\pm\sigma$. (b) Schematic energy level diagram for excitation of light-induced states. Line absorption spectrum measured with overlapped NIR and IAP pulses is shown in black. Peaks in the absorption spectrum around 22, 21.6, and 21.25 eV clearly do not result from excitation to dipole-allowed $1snp$ levels. LISs couple the ground state to $1sns$ and $1snd$ states via absorption of one XUV photon (purple [gray]) and absorption or emission of one NIR photon (red [gray]). (c) Calculated positions of $2s$, $3d$, and $3s$ LISs vs NIR intensity for a delay of -2.7 fs. Full calculations (solid black lines) are compared to three-level model calculations (dashed red [gray] lines).

of an additional NIR photon. For example, the absorption feature at ≈22 eV near zero delay indicates an intermediate state that couples the ground state to the $1s2s$ state. This "$2s$" LIS is located at approximately $\omega_{\mathrm{LIS}} \approx \omega_{1s2s} - \omega_{1s^2} + \omega_{\mathrm{NIR}}$. Similarly, LISs correlated to the $1s3d$ and $1s3s$ states are located approximately one NIR photon below these states at 21.6 and 21.25 eV, respectively. These experiments can thus be thought of in analogy to stimulated Raman spectroscopy studies of atoms [24], but with broadband NIR and XUV pulses. Typical stimulated Raman transitions are two-photon processes where the difference between frequencies of Raman pump and probe pulses is chosen to be resonant with a transition in the target media [25]. In the present case this resonance condition is automatically satisfied in a relatively narrow band of XUV frequencies, picked out of the broadband IAP continuum.

The case for this absorption mechanism can be strengthened by examining the calculations presented in Fig. 2 in more detail. A simple check is provided by repeating the calculations in Fig. 2 while using a TDSE time propagation routine that dynamically eliminates the $1s2s$, $1s3d$, and $1s3s$ states by projecting them out at each time step. As shown in Fig. 4(a), this eliminates the LIS features and causes the $1s2p$ absorption line to become an unshifted, delay-independent feature, in contrast to the full result in Figs. 2(b) and 2(d). This shows that the splitting and shifting of the $1s2p$ state are dominated by NIR-induced couplings to the nearby ns and nd states. In addition, if the LISs are related to processes that couple the ground state to dipole forbidden states, then the strength of the LISs should be related to the population in those states at the end

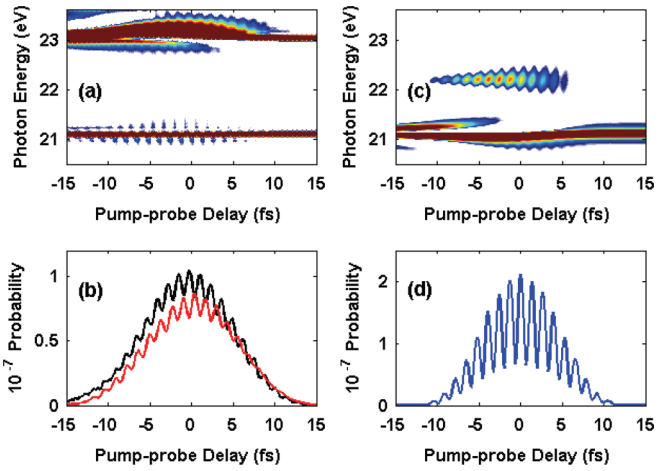

FIG. 4. (Color online) (a) Same as Fig. 2(b) but with the $1s2s$, $1s3s$, and $1s3d$ states all subtracted out during the time propagation. (b) Calculated integrated absorption probability around the 22.2-eV LIS in Fig. 2(b) (black) and the final $2s$ population (red [gray]) vs the pump-probe delay. (c) Three-level model of the response function $\tilde{S}(\omega)$ near the $2s$ LIS with the $1s^2$, $1s2p$, and the $1s2s$ states included. The XUV and NIR pulses are the same as in the full calculations in Fig. 2(b). (d) The $1s2s$ population at the end of the pulses in the three level model of part (c). Note that the units in panels (b) and (d) are the same, without any modification of the original data.

of the laser pulse. As an example, Fig. 4(b) compares the final population in the $1s2s$ state to the calculated integrated absorption around 22.2 eV (the $2s$ LIS). This comparison is straightforward because $\tilde{S}(\omega)$ is a probability per unit frequency, which means that the integrated response in a range of frequencies $\Delta\omega$ around the LIS can be directly compared to the population in a given bound state at the end of the pulse. The calculations show that when (and only when) the $2s$ LIS is observed, population is efficiently transferred to the $1s2s$ state after the pulses have passed. Likewise, the delay-dependent final population in the $1s3d$ and $1s3s$ states follow the strengths of the $3d$ and $3s$ LISs. Taken together, these results support the explanation of the LISs outlined in Fig. 3(b).

The second-order process that gives rise to the $2s$ LIS is the simplest example of the proposed absorption mechanism. The transfer of population from the $1s^2$ ground state to the $1s2s$ state is enabled by the presence of the nearby $1s2p$ state, which has a strong dipole coupling to both states. Solving the TDSE using just these three states is thus helpful for interpreting the absorption data shown in Fig. 2, using the same laser parameters as the full calculation: A peak Rabi frequency of 170 THz (0.7 eV) and a detuning, $\Delta_{2s} = \omega_{\mathrm{NIR}} - \omega_{1s2s-1s2p}$, of 1.1 eV. Figure 4(c) shows that the three-level model (TLM) reproduces the LIS around 22 eV quite well.

Figures 2 and 4 show that both the full calculations and the TLM calculations predict subcycle oscillations in the absorption features when the two pulses are overlapped in time. The modulations happen at twice the laser period and can be seen in both the absorption strengths and the final populations for the $1snp$, $1sns$, and $1snd$ states. These subcycle oscillations are not washed out even though the absorption probability is a time-integrated measure. Using the language of a TLM, one can interpret these oscillations as driven by the counter-rotating terms in the coupling between the $1snp$ and the $1sns$ or $1snd$ states (they are absent in a TLM employing the rotating wave approximation [26]). These counter-rotating terms can be prominent when the NIR Rabi frequency is comparable to the photon energy as in this case [27]. In a true three-level system one would expect these oscillations to be $\pi/2$ out of phase with the driving field because of the large detuning. Indeed, in Figs. 4(c) and 4(d) both the $2s$ LIS absorption and the $2s$ final population peak a quarter cycle after the NIR electric field. In the full calculation, Fig. 4(b), the timing is complicated by the $1s2p$ state interacting with multiple $1sns$ and $1snd$ states, and the LIS absorption does not necessarily peak at the same time as the s and d final-state populations. A full description of these subcycle features is beyond the scope of this paper.

Returning to the experimental data in Figs. 2(a), 2(c), and 3(a), we see that as the NIR intensity is increased, the strength of absorption of the $2s$ LIS near 22 eV increases significantly, whereas those of the $3d$ and $3s$ LISs decrease slightly. This is observed in the calculations in Figs. 2(b) and 2(d) as well. Both the experimental and theoretical results in Fig. 2 also show that the central energy of the LISs can change with NIR delay. The calculations suggest that this is due to the change in NIR intensity with delay. This intensity dependence is studied further in Fig. 3(c) which shows calculations of the central energies of the $2s$, $3d$, and $3s$ LISs as a function of NIR intensity, at a delay of -2.7 fs (solid lines). The experimental intensities are limited to the lower energy portion of the intensity range studied in Fig. 2(c). To better understand the changes in the LIS absorption energy and strength, the full calculations in Fig. 2(c) are compared to TLM calculations constructed separately for each LIS as was done for the $2s$ LIS above. These show that the changes are qualitatively explained by the degree of field detuning involved in each LIS. For example, the $2s$ LIS, which has the largest detuning (1.1 eV) from the NIR laser wavelength, is barely visible in low-intensity data, consistent with a resonant absorption picture where transition strength decreases as detuning increases. The large detuning of the $2s$ LIS also explains why the NIR intensity has little effect on its energy. On the other hand, the central energies of the $3d$ and $3s$ LISs have a much larger dependence on the NIR intensity due to the smaller detunings involved. Note, however, that the intensity dependence of the $3d$ and $3s$ LISs in the full calculation is much bigger than that predicted by the TLM. The TLMs of these LISs break down because the $1s3d$ and $1s3s$ states are resonantly coupled by the NIR field to states near threshold, and these additional couplings cannot be ignored when calculating the position of the LISs. This sensitivity to the NIR intensity can be exploited to make accurate measurements of the LIS properties, to control nondipole coupled-state populations, and to better understand the behavior of these states in a strong NIR field.

In summary, modifications of He atomic absorption spectra are observed in measurements using IAPs in an attosecond transient absorption instrument. The dressed absorption features include LISs, which can be interpreted in terms of second-order resonant transitions to nondipole coupled atomic states. These absorption features can be thought of in analogy to stimulated Raman spectroscopy studies of

atoms [24], and they are observed here in the domain of attosecond spectroscopy. The use of broadband, coherent XUV radiation allows the observation of LISs without specifically tuning to a two-photon transition as would be required with narrowband XUV light. Because the resonance condition is automatically satisfied regardless of the precise NIR frequency, this stimulated absorption technique can be used to study the strong field coupling of excited states in systems more complicated than the simple atomic system used in this study. Both experiment and theory indicate that the properties of the observed LISs can be controlled by varying the NIR intensity and/or the NIR-IAP delay.

This work was supported by the National Science Foundation through Grants No. PHY-0701372 and No. PHY-1019071 and by the Office of Science, Office of Basic Energy Sciences, Chemical Sciences, Geosciences, and Biosciences Division of the US Department of Energy under Contract No. DE-AC02-05CH11231. High-performance computing resources were provided by the Louisiana Optical Network Initiative (LONI). M.J.B. and A.R.B. each acknowledge support from the National Science Foundation. S.R.L. acknowledges support of the NSSEFF. The authors thank T. Pfeifer for helpful discussions and thank the LBNL Center for X-ray Optics (CXRO) for custom-made multilayer mirrors.

[1] E. Goulielmakis, Z-H. Loh, A. Wirth, R. Santra, N. Rohringer, V. S. Yakovlev, S. Zherebtsov, T. Pfeifer, A. M. Azzeer, M. F. Kling, S. R. Leone, and F. Krausz, Nature (London) **466**, 739 (2010).

[2] H. Wang, M. Chini, S. Chen, C. H. Zhang, Y. Cheng, F. He, Y. Cheng, Y. Wu, U. Thumm, and Z. Chang, Phys. Rev. Lett. **105**, 143002 (2010).

[3] R. Santra, V. S. Yakovlev, T. Pfeifer, and Z.-H. Loh, Phys. Rev. A **83**, 033405 (2011).

[4] W.-C. Chu and C. D. Lin, Phys. Rev. A **85**, 013409 (2012).

[5] J. Qi, G. Lazarov, X. Wang, L. Li, L. M. Narducci, A. M. Lyyra, and F. C. Spano, Phys. Rev. Lett. **83**, 288 (1999).

[6] T. E. Glover, M. P. Hertlein, S. H. Southworth, T. K. Allison, J. van Tilborg, E. P. Kanter, B. Krässig, H. R. Varma, B. Rude, R. Santra, A. Belkacem, and L. Young, Nat. Phys. **6**, 69 (2010).

[7] M. Fleischhauer, A. Imamoglu, and J. P. Marangos, Rev. Mod. Phys. **77**, 633 (2005).

[8] P. Johnsson, J. Mauritsson, T. Remetter, A. L'Huillier, and K. J. Schafer, Phys. Rev. Lett. **99**, 233001 (2007).

[9] N. Shivaram, H. Timmers, X.-M. Tong, and A. Sandhu, Phys. Rev. Lett. **108**, 193002 (2012).

[10] M. Holler, F. Schapper, L. Gallmann, and U. Keller, Phys. Rev. Lett. **106**, 123601 (2011).

[11] S. Chen, K. J. Schafer, and M. B. Gaarde, Opt. Lett. **37**, 2211 (2012).

[12] P. Ranitovic, X. M. Tong, B. Gramkow, S. De, B. DePaola, K. P. Singh, W. Cao, M. Magrakvelidze, D. Ray, I. Bocharova, H. Mashiko, A. Sandhu, E. Gagnon, M. M. Murnane, H. C. Kapteyn, I. Litvinyuk, and C. L. Cocke, New J. Phys. **12**, 013008 (2010).

[13] X. M. Tong, P. Ranitovic, C. L. Cocke, and N. Toshima, Phys. Rev. A **81**, 021404 (2010).

[14] M. Chini, B. Zhao, H. Wang, Y. Cheng, S. X. Hu, and Z. Chang, Phys. Rev. Lett. **109**, 073601 (2012).

[15] H. Mashiko, M. J. Bell, A. R. Beck, M. J. Abel, P. M. Nagel, C. P. Steiner, J. Robinson, D. M. Neumark, and S. R. Leone, Opt. Express **18**, 25887 (2010).

[16] H. Mashiko, S. Gilbertson, C. Li, E. Moon, and Z. Chang, Phys. Rev. A **77**, 063423 (2008).

[17] F. Quéré, Y. Mairesse, and J. Itatani, J. Mod. Opt. **52**, 339 (2005).

[18] Y. Mairesse and F. Quéré, Phys. Rev. A **71**, 011401 (2005).

[19] C. Iaconis and I. A. Walmsley, IEEE J. Quantum Electron. **35**, 501 (1999).

[20] D. Kane, IEEE J. Quantum Electron. **35**, 421 (1999).

[21] D. J. Tannor, *Introduction to Quantum Mechanics: A Time-Dependent Perspective* (University Science Books, Sausalito, CA, 2007).

[22] M. B. Gaarde, C. Buth, J. L. Tate, and K. J. Schafer, Phys. Rev. A **83**, 013419 (2011).

[23] C. H. Brito Cruz, J. P. Gordon, P. C. Becker, R. L. Fork, and C. V. Shank, IEEE J. Quantum Electron. **24**, 261 (1988).

[24] P. P. Sorokin, N. S. Shiren, J. R. Lankard, E. C. Hammond, and T. G. Kazyaka, Appl. Phys. Lett. **10**, 44 (1967).

[25] P. Kukura, D. W. McCamant, and R. A. Mathies, Annu. Rev. Phys. Chem. **58**, 461 (2007).

[26] A. N. Pfeiffer and S. R. Leone, Phys. Rev. A **85**, 053422 (2012).

[27] L. Allen and J. H. Eberly, *Optical Resonance and Two-Level Atoms* (Courier Dover, New York, 1987).